Journal of Alloys and Compounds, 187 (1992) 305–315
JALCOM 335

Exchange reaction milling in iron nitrides, fluorides and carbides

Paolo Matteazzi
Dipartimento di Scienze e Tecnologie Chimiche, Università degli Studi di Udine, Via Cotonificio 108, I-33100 Udine (Italy)

Gerard Le Caër
Laboratoire de Science et Génie des Matériaux Métalliques Associé au CNRS URA 159, Ecole des Mines, F-54042 Nancy Cédex (France)

(Received March 18, 1992)

Abstract

Solid state room temperature exchange reactions of iron nitride, fluoride and cementite with silicon or aluminium, carbon and chromium respectively are described. Reactions are driven by ball milling powder mixtures of the compound and the exchange element at room temperature. In the different systems the formation of Si_3N_4, AlN, carbon fluorides and an amorphous (Fe,Cr)C alloy is observed. Nanocomposite materials are synthesized in this way. X-ray diffraction and Mössbauer spectroscopy were used to characterize the powders before and after processing.

1. Introduction

The mechanochemical synthesis (mechanosynthesis) of a wide group of compounds such as carbides [1], intermetallic compounds (silicides, aluminides, stannides, etc.) [2, 3], borides [4] and nitrides [5–7] has been shown to be feasible by ball milling of elemental powders for a few hours at room temperature. More recently, solid state reduction reactions of oxides [8, 9] and sulphides [10] were performed by mechanical activation. Materials obtained in this way are nanophased (crystallite sizes around 10–20 nm) and often nanocomposites [9].

In the present paper we investigate the possibility of performing exchange or displacement of nitrogen, fluorine and carbon contained in iron nitride, fluoride and cementite milled with silicon or aluminium, carbon and chromium respectively. We choose to investigate iron-containing compounds so that we follow the transformations also by Mössbauer spectroscopy.

2. Experimental details

We performed experiments according to the following generic reaction schemes:

0925-8388/92/$5.00

$$\text{(iron nitride)} + \text{Al} \longrightarrow \text{AlN} + \text{Fe} \quad (1)$$

$$\text{(iron nitride)} + \text{Si} \longrightarrow \text{Si}_3\text{N}_4 + \text{Fe} \quad (2)$$

$$\text{FeF}_3 + \text{C} \longrightarrow \text{C}_{\text{fluoride}} + \text{Fe}_{\text{fluoride}} \quad (3)$$

$$\text{Fe}_3\text{C} + \text{Cr} \longrightarrow (\text{Fe,Cr})_{\text{carbide}} \quad (4)$$

The experiments were performed in a vibratory ball mill (Spex 8000 mixer–mill) using WC vial and balls. The starting materials were powders of the compound and the element (reactions (1)–(4)), which were introduced into the vial in the required proportions and sealed in a glove-box under a pure nitrogen atmosphere. In the paper we will define p-A_aB_b as the initial mixture of powders of A (compound) and B (element) in the atomic ratio a:b. Milling has been performed for all the experiments for a time long enough (24 h) generally to assess the feasibility of the reaction. The powders of the elements had a purity of 99% or more and average particle sizes of 30–70 μm.

The milled products have been characterized by ^{57}Fe Mössbauer spectroscopy (for iron-containing systems) and X-ray diffraction (XRD).

^{57}Fe Mössbauer spectroscopy was employed in the transmission geometry using a source of ^{57}Co in a rhodium matrix at room temperature. Isomer shifts (δ) are referred to α-Fe and the quadrupole splitting ϵ is defined as half the total splitting.

XRD patterns were collected using an INEL diffractometer equipped with a CPS-120 position-sensitive detector and a germanium monochromator using Co Kα ($\lambda = 0.1789$ nm) radiation.

3. Results

3.1. Milling of iron nitrides with aluminium and silicon

The Mössbauer spectrum of the starting iron nitride powder (mean size 15 μm), reported in Fig. 1(A), shows the presence of the following hyperfine components.

(1) Two broad magnetic components with $H = 203$ and 107 kG, $\delta = 0.31$ and 0.41 mm s^{-1} and relative area percentage %RA = 32 and 41 respectively. The variation in the Curie temperature of iron nitrides as a function of nitrogen content shows a maximum at about Fe_3N [11]. It is therefore possible to interpret the maximum field of 203 kG either as being due to iron(I) with only one nitrogen nearest neighbour in a nitrogen-poor nitride, approximately $Fe_{4\pm0.2}N$, using the relative areas [12] or as being due to iron(II) atoms with two nearest neighbours. The isomer shift values at room temperature favour the second interpretation. A simple relation which again uses the %RA and extends a relation given in ref. 12 correlating site abundances with nitrogen content allows us to calculate the composition $Fe_{2.34}N$. A direct comparison of the hyperfine fields with those published by Chen *et al.* [13]

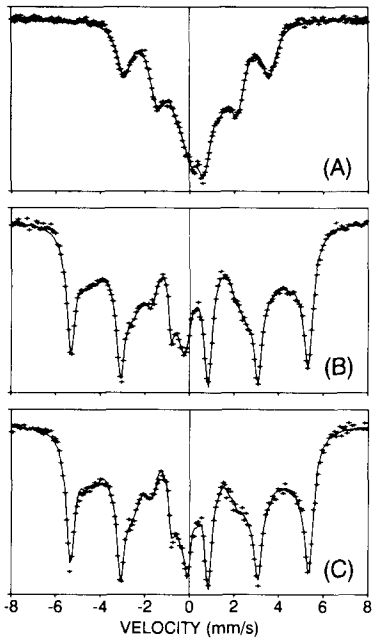

Fig. 1. Mössbauer spectra of (A) starting iron nitride ($Fe_{2.5}N$), (B) milled p-($Fe_{2.5}N$)Al_2 and (C) milled p-($Fe_{2.5}N$)$Si_{4/3}$.

allows us to conclude that the nitrogen content in Fe_xN is close to $x=2.67$ (fields of 205 and 100 kG at room temperature with isomer shifts values of 0.34 and 0.40 mm s^{-1} respectively).

(2) A paramagnetic component (%RA=27) with $\delta=0.38$ mm s^{-1} and $\epsilon=0.27$ mm s^{-1}, attributed to $Fe_{2+y}N$ ($y<0.2$) according to ref. 14.

Assuming that the two components have the same f factors, then the starting iron nitride has an average composition approximately $Fe_{2.5}N$, in satisfactory agreement with the approximate composition $Fe_{2.3}N$ deduced from the relative areas, neglecting the differences in the Debye–Waller factors of the various sites.

We milled a powder mixture p-($Fe_{2.5}N$)Al_2 using a powder-to-ball (PB) weight ratio PB=1:10 to perform reaction (1). The XRD pattern in Fig. 2(A) shows the presence of sharp peaks due to WC contamination from the grinding method, and broad peaks, the most intense of which, located at around $2\theta=50°$, can be partly attributed to the formation of cubic AlN with a lattice parameter $a=0.4130\pm0.0012$ nm (in agreement with the value reported in JCPDS card 25-1495 [15], $a=0.412$ nm). Other components of the pattern are: hexagonal AlN (JCPDS 25-1133); iron (an $Fe_{1-x}Al_x$ alloy according to the Mössbauer analysis below); hexagonal Fe_xN (JCPDS 1-1236). Aluminium lines are not present and therefore the aluminium reacted completely with the starting iron nitride. The XRD line broadening was evaluated according to the method described in ref. 2 to extract the crystallite sizes for cubic AlN (8 ± 1 nm) and $Fe_{1-x}Al_x$ (9 ± 1 nm).

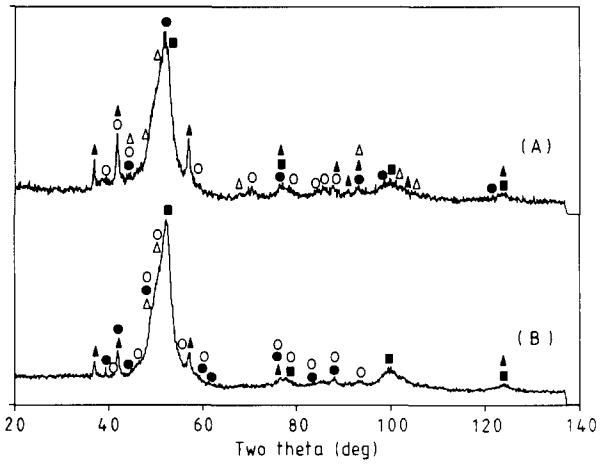

Fig. 2. X-ray diffraction patterns of (A) milled p-($Fe_{2.5}N$)Al_2 and (B) milled p-($Fe_{2.5}N$)$Si_{4/3}$. Symbols are: iron (■), WC (▲), hexagonal Fe_xN (△); (A) cubic AlN (●), hexagonal AlN (○); (B) JCPDS 33-1160 Si_3N_4 (●), JCPDS 9-250 Si_3N_4 (○).

Consideration of the Mössbauer spectrum in Fig. 1(B) allows a more detailed analysis of the iron compounds formed. The spectrum consists of a paramagnetic component and several (broad) magnetic components with $H=333$, 292, 254 and 215 kG, $\delta=0.02$, 0.14, 0.22 and 0.24 mm s^{-1} and %RA = 33, 15, 15 and 13 respectively. Both the hyperfine field and isomer shift values are consistent with the presence of a heterogeneous $Fe_{1-x}Al_x$ alloy [16]. The average composition of such an alloy as estimated from the mean hyperfine field ($H_a=287$ kG) is $x=0.21$ [16].

Further magnetic components are present, but the corresponding peaks are strongly overlapped both by the peaks of the $Fe_{1-x}Al_x$ alloy and by the central paramagnetic component. Nevertheless, a component with $H=183$ kG, $\delta=0.31$ mm s^{-1} and %RA = 13 can be derived from the fitting. Another component with a small field ($H=67$ kG, $\delta=0.46$ mm s^{-1}, %RA = 3) is probably underestimated. Both may be interpreted as coming from a hexagonal iron nitride, approximately $Fe_{2.4-2.5}N$ ($H=186$ kG for iron(II) at room temperature in $Fe_{2.47}N$ and 84 kG for iron(III) with three nitrogen nearest neighbours [13]). The latter result is consistent with the initial average nitrogen content, since we expect that the non-reacted nitrides will mix together to give a unique hexagonal nitride with the average nitrogen content [5, 6].

The paramagnetic component (%RA = 8), interpreted as a doublet, has hyperfine parameters $\delta=0.18$ mm s^{-1} and $\epsilon=0.28$ mm s^{-1} and may be tentatively ascribed to the presence of an aluminium rich Fe–Al compound close to Al_5Fe_2 [17].

If we assume that all the initial nitrogen is still in the reaction products and that all the f factors are the same, then the path of reaction (1) can

be described from the XRD and Mössbauer results as approximately

$$Fe_{2.5}N + 2Al \longrightarrow 0.84\ AlN + 0.16Fe_{2.5}N + 2.4Fe_{0.79}Al_{0.21} + 0.12Fe_2Al_5$$

The initial aluminium excess employed has led therefore, together with aluminium nitride, to Fe–Al alloys that have formed from the aluminium by mechanical alloying with metallic iron.

Milling of p-$(Fe_{2.5}N)Si_{4/3}$ was performed under PB = 1:10 conditions. The XRD pattern in Fig. 2(B), similarly to the previous case, shows the presence of WC peaks and phases corresponding to reaction (2) products, namely: iron (an Fe–Si alloy; see below); hexagonal β-Si_3N_4 crystallizing in the space group $P63/m$ with $a = 0.7610 \pm 0.0064$ nm and $c = 0.2844 \pm 0.0039$ nm (JCPDS 33-1160 gives $a = 0.76044$ nm and $c = 0.29075$ nm); hexagonal Si_3N_4 crystallizing in the space group $P31c$ with lattice parameters $a = 0.7738 \pm 0.0072$ nm and $c = 0.5608 \pm 0.0033$ nm (JCPDS 9-250 gives $a = 0.7758$ nm and $c = 0.5623$ nm) and crystallite size (by the method described in ref. 2) 22 ± 4 nm; hexagonal Fe_xN (JCPDS 1-1236).

The Mössbauer spectrum in Fig. 1(C), similarly to the previous case, shows the presence of a paramagnetic component and several magnetic components. The latter have been identified to have $H = 332$, 301, 279 and 254 kG, $\delta = 0.02$, 0.14, 0.13 and 0.18 mm s^{-1} and %RA = 34, 9, 9 and 8 respectively. These hyperfine field and isomer shift values can be attributed to iron atoms perturbed by the presence of silicon atoms in the next-neighbour shell, as shown in ref. 18. The average hyperfine field ($H_a = 309$ kG) allows us to estimate the composition of the $Fe_{1-x}Si_x$ alloy formed as $x = 0.20$ according to the concentration dependence reported in ref. 19 for crystalline Fe–Si alloys. As in the previous case, two further magnetic components are found with $H = 210$ and 71 kG, $\delta = 0.24$ and 0.59 mm s^{-1} and %RA = 23 and 11 respectively. These belong to hexagonal ϵ-Fe_xN with $x \approx 2.6 \pm 0.1$, in agreement with the previous discussion.

The paramagnetic component consists of a doublet with $\delta = 0.10$ mm s^{-1}, $\epsilon = 0.19$ mm s^{-1} and %RA = 6 and can be attributed to β-$FeSi_2$ according to the hyperfine parameters reported in ref. 20.

In analogy with the previous case and with identical assumptions, we may write the reaction path (2), taking into account the XRD and Mössbauer results, as approximately

$$Fe_{2.5}N + 1.3Si \longrightarrow 0.17Si_3N_4 + 0.34Fe_{2.5}N + 1.9Fe_{0.8}Si_{0.2} + 0.2FeSi_2$$

Also in this case the formation of silicon nitrides is accompanied by Fe–Si alloys and compounds that have formed from mechanical alloying of the excess silicon with iron. This demonstrates that an exchange reaction of type (2) clearly occurred.

3.2. Milling of FeF_3 with carbon

The Mössbauer spectrum of the initial iron fluoride (FeF_3, 99%, 20 μm) is presented in Fig. 3(A). The spectrum has been fitted by using a hyperfine

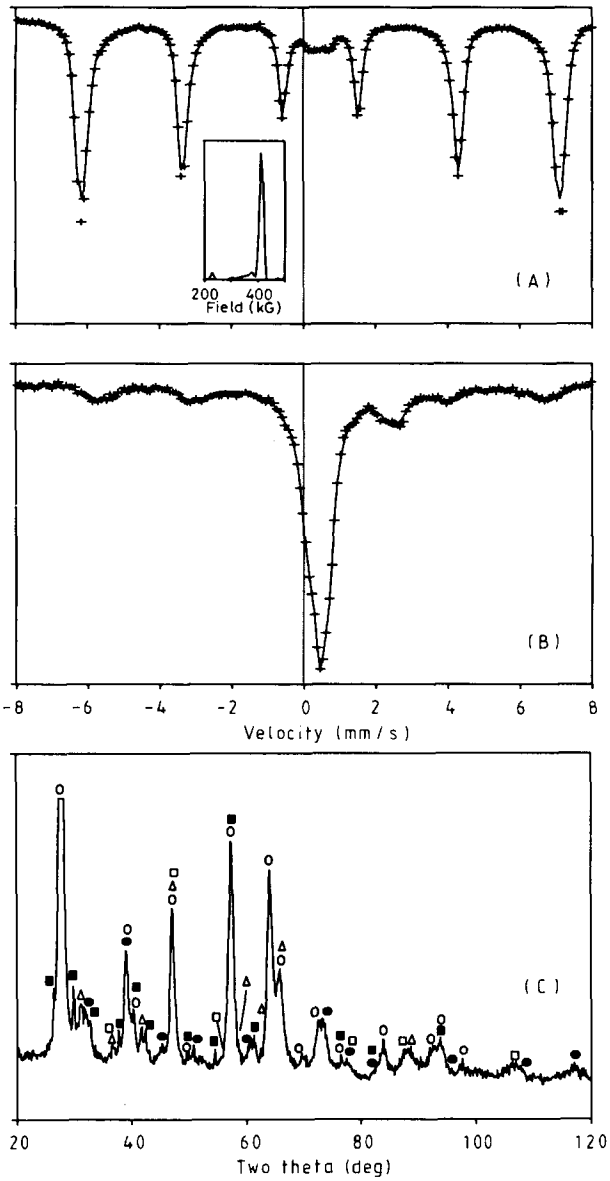

Fig. 3. Mössbauer spectra of (A) starting iron fluoride (FeF_3), (inset: the hyperfine field distribution) and (B) milled p-$(FeF_3)C_{3/4}$. (C) X-ray diffraction pattern of milled p-$(FeF_3)C_{3/4}$. Symbols are: tetragonal FeF_2 (●), rhombohedral FeF_3 (○), tetragonal β-$FeF_3 \cdot 3H_2O$ (■), poly carbon fluoride $(CF)_n$ (△), carbon fluoride $(CF_{1.1})_n$ (□).

field distribution (HFD) with an average isomer shift $\delta = 0.48$ mm s^{-1} (100–500 kG), together with a paramagnetic component with $\delta = 0.45$ mm s^{-1} and $\epsilon = 0.19$ mm s^{-1}. The HFD (inset in Fig. 3(A)) showed the presence of a narrow peak with a field having a maximum probability at $H = 410$ kG, which

is in good agreement with previously reported hyperfine parameters for FeF_3 [21]. The paramagnetic component (%RA = 5) most probably arises from α-$FeF_3 \cdot 3H_2O$, since both the isomer shift and quadrupole splitting are consistent with those reported in ref. 22 and 23.

Reaction scheme (3) was performed by milling p-$(FeF_3)C_{3/4}$ using PB = 1:14. The Mössbauer spectrum in Fig. 3(B) shows that a strong modification of the ^{57}Fe environment occurred after milling. The following components, in agreement with the XRD results, were identified.

(1) A broad magnetic (full linewidth $\Gamma = 0.9$ mm s^{-1}) component (%RA = 25) with $H = 383$ kG and $\delta = 0.52$ mm s^{-1} arising from FeF_3. The reduced value of the hyperfine field can be justified by taking into account that a reduced Néel temperature was observed in FeF_3 thin films [24] owing to the presence of defects. Both this and the small crystal sizes may determine the large linewidth observed [24].

(2) A paramagnetic component (%RA = 21) with $\delta = 1.48$ mm s^{-1} and $\epsilon = 1.03$ mm s^{-1}. According to Ramasamy *et al.* [25], these hyperfine parameters may correspond to iron atoms in FeF_2 at grain boundaries, although we were not able to identify any 'bulk' component (with larger quadrupole splitting, *i.e.* $\epsilon \approx 1.35$ mm s^{-1}).

(3) A paramagnetic component (%RA = 54) with $\delta = 0.42$ mm s^{-1} and $\epsilon = 0.24$ mm s^{-1}, which are close to the hyperfine parameters given in ref. 26 for hydrated $FeF_3 \cdot (H_2O)_{0.33}$.

The XRD pattern in Fig. 3(C) leads to the identification of the following phases, confirming also the Mössbauer results: tetragonal FeF_2 (JCPDS 18-638); rhombohedral FeF_3 (JCPDS 33-647); tetragonal β-$FeF_3 \cdot 3H_2O$ (JCPDS 32-464); poly carbon fluoride $(CF)_n$ and carbon fluoride $(CF_{1.1})_n$ according to the reference data in JCPDS cards 27-1873 and 30-476 respectively.

3.3. Milling of Fe_3C with chromium

The initial Fe_3C (Strem Chemicals Inc., 99.9%, 30 μm) was constituted, as proved by Mössbauer spectroscopy, by about 6.5% α-Fe, 84% Fe_3C and 10% of an ϵ-carbonitride.

We have shown in previous cases that the mechanosynthesis of mixed carbides from the elemental powders is feasible [1]. In this experiment the purpose was to verify if mixed carbides can be obtained by the reaction of an already formed carbide with a metal as in reaction (4). For this purpose we milled p-$(Fe_3C)Cr_{7/3}$ using PB = 1:8.

The XRD pattern of the milled powder in Fig. 4(A) shows the presence of WC lines, a residual amount of chromium (weak lines) and two broad peaks located at $2\theta = 45°$–$60°$ (more intense) and $2\theta = 85°$–$105°$. Amorphous $Fe_{1-x}C_x$ [27] and amorphous $Cr_{1-x}C_x$ [28] also show broad peaks in the same 2θ angular ranges, *i.e.* 45°–60° and 85°–105°. The positions of lines for the carbides $Cr_{23}C_6$ (JCPDS 35-783) and $(Cr,Fe)_7C_3$ (JCPDS 5-720) are also shown.

The Mössbauer spectrum shown in Fig. 4(B) clearly reveals that the original Fe_3C (which has a magnetically split spectrum with $H = 205$ kG)

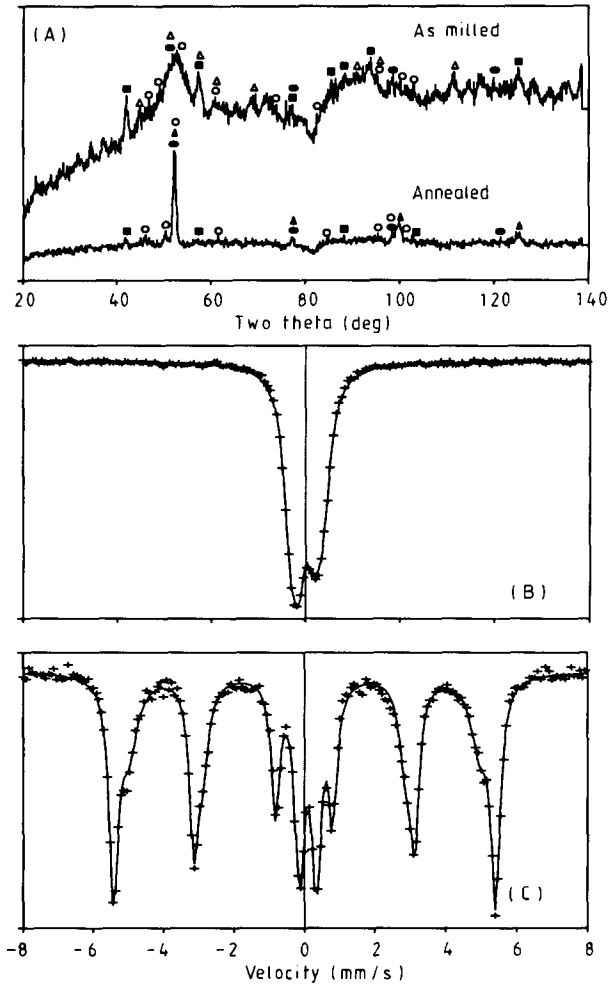

Fig. 4. Milling of p-$(Fe_3C)Cr_{7/3}$. (A) X-ray diffraction patterns of as-milled and annealed powders. Symbols are: iron (▲), chromium (●), $(Cr,Fe)_7C_3$ (○), $Cr_{23}C_6$ (△), WC (■). Mössbauer spectra of (B) as-milled and (C) annealed powders.

has been transformed, since the only component is a paramagnetic peak. The latter can be fitted with two doublets with $\delta = 0.00$ and 0.01 mm s^{-1}, $\epsilon = 0.16$ and 0.35 mm s^{-1} and %RA = 58 and 42 respectively. This paramagnetic component is consistent either with a mixed Fe–Cr carbide with very small crystallite sizes in order to account for the broad XRD lines or with an amorphous (Fe–Cr)C alloy with a carbon content of the order of 18 at.% C.

Differential thermal analysis performed on the as-milled powder showed an exothermic transformation at about 530 °C. The XRD pattern of the

annealed powder (Fig. 4(A)) reveals that a transformation of the two broad peaks has occurred. The chromium and iron lines are clearly detected together with a residual amount of $(Cr,Fe)_7C_3$ carbide (the presence of a small amount of an $(Fe,Cr)_3C$ carbide cannot be excluded, owing to overlapping lines both to the former carbide and to iron lines).

Mössbauer spectroscopy on the powder after thermal analysis, *i.e.* annealed (Fig. 4(C)), shows the formation of an Fe–Cr alloy with a magnetically split spectrum (two magnetic components with $H = 337$ and 310 kG, $\delta = 0.00$ and -0.01 mm s^{-1} and %RA = 46 and 32 respectively) and residual amounts of a mixed (Fe,Cr) carbide, giving rise to a doublet with $\delta = 0.10$ mm s^{-1}, $\epsilon = 0.24$ mm s^{-1} and %RA = 22. The hyperfine parameters of the two magnetic subspectra are in perfect agreement with published values for $Fe_{1-x}Cr_x$ alloys [29]. It is possible to estimate the chromium content of the alloy as $x \approx 0.03$. This means that almost all the chromium combined with iron is in the carbide which gives rise to the central peak. The latter carbide is therefore chromium rich: an evaluation using the relative areas gives $x \approx 0.75$ in $(Fe_{1-x}Cr_x)_yC_z$. It is difficult to know whether the latter carbide is composed only of the $(Fe,Cr)_7C_3$ carbide or also of a cementite-type carbide $(Fe,Cr)_3C$ (a cementite Cr_3C carbide is not a stable phase but is metastable and can be obtained either by rapid quenching or by crystallization of low carbon content amorphous Cr–C alloys [28, 30, 31]).

The simultaneous observation of broad XRD lines and a single broadened Mössbauer doublet in the as-milled material together with an (Fe,Cr) alloy and a residual carbide after annealing is consistent with the hypothesis that most of the as-milled material consists of an amorphous $(Fe–Cr_{rich})C$ phase with a carbon content below about 20 at.%.

4. Conclusions

Several exchange, transfer and mixing reactions can be driven by mechanical activation in the solid state at room temperature.

In previous experiments we reported mechanically driven reactions involving: transfer of oxygen (reduction of oxides [9]); transfer of sulphur (reduction of sulphides) [10]; exchange of both sulphur and oxygen by reaction milling of CaO and metal sulphides [10].

In the present paper we obtained a partial transfer of nitrogen from iron nitride to aluminium and silicon, with the formation of aluminium and silicon nitrides respectively. Partial transfer of fluorine was obtained by reaction milling of iron fluorides with carbon, resulting in the formation of carbon fluorides. The formation of a mixed, largely amorphous (Fe,Cr)C alloy was obtained after milling iron cementite and chromium.

The milled powders obtained have low crystallite sizes (10–20 nm) and can be classified as nanocomposites constituted of $AlN–Fe_{2.5}N–(FeAl)_{alloy}$, $Si_3N_4–Fe_{2.5}N–(FeSi)_{alloy}$, $FeF_3–FeF_2–FeF_3 \cdot (H_2O)_{0.33}–(CF)_n–(CF_{1.1})_n$ and $(Fe,Cr)_{carbide}–(Fe,Cr)C_{amorphous\ alloy}$ respectively.

Acknowledgment

The financial contribution of the European Economic Community with grant SC1-CT91-0668 (Science Program), which partially supported the work, is gratefully acknowledged.

References

1 P. Matteazzi and G. Le Caër, Room temperature mechanosynthesis of carbides by grinding of elemental powders, *J. Am. Ceram. Soc., 74* (6) (1991) 1382–1390.
2 P. Matteazzi and G. Le Caër, Synthesis of nanocrystalline intermetallic compounds by room temperature ball milling of the elemental powders, *Proc. Adv. Mater., 1* (1992) 135.
3 M. Atzmon, *In situ* thermal observation of explosive compound-formation reaction during mechanical alloying, *Phys. Rev. Lett., 64* (4) (1990) 487–490.
4 A. Calka and A. P. Radlinski, Formation of TiB_2 by mechanical alloying, *J. Less-Common Met., 161* (1990) L23–L26.
5 P. Rochegude and J. Foct, Comportement de l'azote lors de la mise en alliage par broyage mécanique de solutions solides et de nitrures de fer et d'éléments de transition voisins, *C.R. Acad. Sci. Paris, Ser. II, 309* (1989) 1545–1549.
6 J. Foct and A. Mastorakis, High nitrogen steels and nitrides obtained by mechanical alloying, personal communication, 1992.
7 A. Calka, Formation of titanium and zirconium nitrides by mechanical alloying, *Appl. Phys. Lett., 59* (13) (1991) 1568–1569.
8 G. B. Schaffer and P. G. McCormick, Displacement reactions during mechanical alloying, *Metall. Trans. A, 21* (1990) 2789–2794.
9 P. Matteazzi and G. Le Caër, Synthesis of nanocrystalline alumina–metal composites by room temperature ball milling of metal oxides and aluminium, *J. Am. Ceram. Soc.*, in the press.
10 P. Matteazzi and G. Le Caër, Mechanically activated room temperature reduction of sulphides, *Mater. Sci. Eng.*, in the press.
11 N. DeCristofaro and R. Kaplow, Mössbauer spectroscopy of hexagonal iron–nitrogen alloys, *Metall. Trans. A, 8* (1977) 425–430.
12 J. Foct, Etude par spectrométrie Mössbauer de la distribution des interstitiels dans le nitrure de fer hexagonal au voisinage de la composition Fe_4N, *C.R. Acad. Sci. Paris, Ser. C, 276* (1973) 21–24.
13 G. M. Chen, N. K. Jaggi, J. B. Butt, E. B. Yeh and L. H. Schwartz, Mössbauer and magnetic studies of ϵ-Fe_xN, $2 < x < 3$, *J. Phys. Chem., 87* (1983) 5326–5332.
14 E. Yeh, N. K. Jaggi, J. B. Butt and L. Schwartz, Silica-supported iron nitride in Fischer–Tropsch reactions, *J. Catal., 91* (1985) 231–240.
15 *JCPDS Powder Diffraction Files PDF-2*, Sets 1–40, Joint Committee on Powder Diffraction Standards, Philadelphia, PA, 1990.
16 S. M. Dubiel and W. Zinn, Mössbauer study of spin and charge density changes in Fe–Al alloys, *Phys. Rev. B, 26* (4) (1982) 1574–1588.
17 T. Birchall, D. Hodgson and H. D. Merchant, The application of Mössbauer spectroscopy to iron–aluminium alloys and industrial aluminium samples, in G. J. Long and J. G. Stevens (eds.), *Industrial Applications of the Mössbauer Effect*, Plenum, New York, 1986, pp. 189–200.
18 M. Arita, A. Nasu and F. E. Fujita, Determination of long-range-order parameter of Fe_3Si alloy by means of ^{57}Fe Mössbauer effect, *Trans. Jpn. Inst. Met., 26* (10) (1985) 710–720.
19 C. Bansal, S. J. Campbell and A. M. Stewart, Mössbauer and magnetic resonance experiments on amorphous iron–silicon films, *J. Magn. Magn. Mater., 27* (1982) 195–201.
20 K. Vojtechovsky and T. Zemcik, Mössbauer study of the Fe–Si intermetallic compounds, *Czech. J. Phys. B, 24* (1974) 171–178.

21 G. K. Wertheim, H. J. Guggenheim and D. N. E. Buchanan, Sublattice magnetization in FeF_3 near the critical point, *Phys. Rev.*, *169* (1968) 465–470.
22 I. Dezsi, S. G. Sankar, L. N. Mulay, J. F. Houlihan and T. Pannaparayil, Magnetic ordering in α- and β-$FeF_3 \cdot 3H_2O$, *J. Phys. (Paris), Colloq. C8, 49* (1988) 1463–1464.
23 N. N. Greenwood and T. C. Gibb, *Mössbauer Spectroscopy*, Chapman and Hall, London, 1971.
24 A. Lachter, J. C. Gianduzzo, A. S. Barriere, L. Fournes and F. Menil, Magnetic and Mössbauer resonance studies of FeF_3 thin films, *Phys. Status Solidi A, 61* (1980) 619–630.
25 S. Ramasamy, J. Jiang, H. Gleiter, R. Birringer and U. Gonser, Investigation of nanocrystalline FeF_2 by Mössbauer spectroscopy, *Solid State Commun.*, *74* (8) (1990) 851–855.
26 Y. Calage, M. Leblanc, G. Ferey and F. Varret, Mössbauer investigation of hexagonal tungsten bronze type Fe^{III} fluorides: $(H_2O)_{0.33}FeF_3$ and anhydrous FeF_3, *J. Magn. Magn. Mater.*, *43* (1984) 195–203.
27 E. Bauer-Grosse and G. Le Caër, Structural evolution of sputtered amorphous iron–carbon ($Fe_{1-x}C_x$) films for $0.19 < x < 0.49$, *Philos. Mag. B, 56* (4) (1987) 485–500.
28 E. Bouzy, Structures et défauts des carbures produits par la crystallization d'alliages amorphes chrome–carbone, *Thesis*, INPL, Nancy, 1991.
29 S. M. Dubiel and J. Zukrowski, Mössbauer effect study of charge and spin transfer in Fe–Cr, *J. Magn. Magn. Mater.*, *23* (1981) 214–228.
30 A. Inoue and T. Masumoto, Formation of nonequilibrium chromium carbide Cr_3C in chromium carbon binary alloys quenched rapidly from the melt, *Scr. Metall.*, *13*(8) (1979) 711–715.
31 M. Naka, S. Hanada and I. Okamoto, Formation and crystallization of Cr–C sputtered amorphous alloys, in S. Steeb and H. Warlimont (eds.), *Rapidly Quenched Metals*, Vol. 1, Elsevier, Amsterdam, 1985, pp. 361–364.